Antibacterial and Antioxidant Efficacy of ZnO and Ag-Doped ZnO Nanoparticles Synthesized Using Artemisia absinthium Leaf Extract: A Comparative Study

Fatima Ahmed Al-Yusufy , Fawzeeh Nayif Alharbi , Zulfa Mohamed Abaker * , Suzan Zein Alabdeen Makawi , Tasneem Ibrahim Hussein , Ebtesam Hassan Lutf Alhamzi

Posted Date: 5 November 2024

doi: 10.20944/preprints202411.0348.v1

Keywords: green synthesis; Ag-doped ZnO NPs; antioxidant activity; DPPH antibacterial activity; gentamycin antibiotic

 doi:10.20944/preprints202411.0348.v1

Article

Antibacterial and Antioxidant Efficacy of ZnO and Ag-Doped ZnO Nanoparticles Synthesized Using *Artemisia absinthium* Leaf Extract: A Comparative Study

Fatima Ahmed Al-Yusufy [1], Fawzeeh Nayif Alharbi [2], Zulfa Mohamed Abaker [1,*], Suzan Zein Alabdeen Makawi [1], Tasneem Ibrahim Hussein [1] and Ebtesam Hassan Lutf Alhamzi [3]

[1] Department of Chemistry, College of Science, Qassium University, Ar Rass 51921, Saudi Arabia
[2] Department of Chemistry, College of Science, Qassim University, Buraidah 51452, Saudi Arabia
[3] Department of Biology, Faculty of Science, Sana'a University, Sana'a, Yemen
* Correspondence: zulfa.abaker@gmail.com

Abstract: An eco-friendly plant-mediated approach was employed for the synthesis of green zinc oxide nanoparticles (ZnO NPs) and silver-doped zinc oxide nanoparticles (Ag-doped ZnO NPs), using *Artemisia Absinthium* leaf extract as a reducing and capping agent. Pure ZnO NPs were also synthesized without the leaf extract, and a comparative study between them was conducted. The nanoparticles (NPs) were characterized using Fourier transform infrared (FTIR) spectroscopy, X-ray diffraction (XRD), morphological scanning electron microscopy/energy dispersive spectrum (SEM/EDX), and surface area (BET) analysis, and antioxidant and antibacterial activity measurements were conducted. The FTIR analysis showed the absorption peak of the Zn–O bond between 400 and 450 cm^{-1}. The XRD analysis revealed that the ZnO NPs had a hexagonal wurtzite structure with a decrease in particle size from 36.32 to 27.40 to 25.13 nm, and an increase in the BET from 4.003 to 6.032 to 12.151 m2/g for the pure, green, and Ag-doped ZnO NPs, respectively. The field emission scanning electron microscopy (FESEM) imaging revealed the presence of the ZnO NPs. The EDX results showed the zinc and oxygen composition exhibited strong energy signals of 71.28% and 18.12% for zinc and oxygen, respectively. The various characterization techniques used confirmed the formation of the ZnO NPs. The free radical scavenging activities (RSA%) measured using the 1,1-diphenyl-2-picrylhydrazyl free radical (DPPH) assay at different concentrations and times for the pure, green, and Ag-doped ZnO NPs, and ascorbic acid were 25.50, 29.27, 28.56, and 56.7, respectively. The antibacterial activity of the synthesized samples was tested against three types of bacteria, *Staphylococcus aureus* ATCC 6538, *Bacillus subtilis* ATCC 6633, and *Pseudomonas aeruginosa* ATCC 9027, at different levels (5, 10, 20, and 30 µL), using the hole plate diffusion method. The Ag/ZnO NPs showed more enhanced antibacterial activity than the green ZnO NPs, whereas the pure ZnO NPs showed no antibacterial activity under the same conditions. Comparatively, the antibacterial activity of the Ag-doped ZnO NPs against the test bacteria was found to be higher than that of a commercial gentamycin antibiotic. Ultimately, the present investigation has clearly shown that the differences in the ZnO NPs' sizes and surface-area-to-volume ratios are responsible for their stronger antibacterial activity.

Keywords: green synthesis; Ag-doped ZnO NPs; antioxidant activity; DPPH antibacterial activity; gentamycin antibiotic

1. Introduction

In recent years, the study of nanoparticles (NPs) has emerged as one of the major basic fields in the biomedical sciences[1]. Among several routes of NP synthesis, the green synthesis method has been reported as an environmentally friendly approach[2].

The majority of plants are naturally capable of reducing and capping a variety of metal and metal oxide NPs, yet some are more capable than others because they contain special phytochemical components that are crucial to the bio-reduction process and the subsequent creation of NPs[3,4].

 doi:10.20944/preprints202411.0348.v1

Zinc oxide nanoparticles (ZnO NPs) have attracted a lot of interest due to their potential medical applications. The results of numerous studies have demonstrated the potent pharmacological characteristics of ZnO NPs, including their antioxidant[5], antibacterial[6], and anti-cancer activity[7].

ZnO NPs' antioxidant activity enables the body to combat free radicals. This type of activity can also be utilized as a preventive measure against degenerative illnesses caused by free radical damage. Atherosclerosis, cancer, stroke, trauma, asthma, heart attacks, arthritis, age-related pigmentation, cataracts, hepatitis, and periodontitis are a few conditions brought on by free radicals[8]. Free radicals are a typical byproduct of cellular metabolism, and they are produced alongside reactive oxygen species on a regular basis in our cells. Disruption of the equilibrium between endogenous defense mechanisms and reactive oxygen species (ROS), or free radicals, is known as oxidative stress. The formation of ROS can increase when in a diseased state[9].

The two primary categories of antioxidant activity measurement techniques are colorimetric and non-colorimetric. The most widely used and straightforward colorimetric techniques are 1,1-diphenyl-2-picrylhydrazyl free radical (DPPH) and ferric reducing antioxidant power (FRAP) assays, whereas the hydroxyl radical scavenging assay (HRSA) is a non-colorimetric technique. The time-effectiveness, affordability, and simplicity of the DPPH assay make it a popular choice. The reaction mechanism in the DPPH assay is based on electron transfer. However, this is based on the scavenging of an organic radical (DPPH radical)[10].

According to recent publications, ZnO NPs have biological uses in medication administration, gene transfer, and bioimprinting. They are also said to possess antibacterial, antifungal, anti-diabetic, and anticorrosive properties[11,12]. Several studies have been conducted on the remarkable antibacterial properties of ZnO and silver NPs alone, but very few on the antibacterial properties of silver-doped ZnO NPs (Ag-doped ZnO NPs) have been conducted.

Green ZnO NPs and Ag-doped ZnO NPs are better than conventional antibiotics because they affect bacteria directly through a variety of mechanisms, including bacterial cell membrane penetration; bacterial cell disruption; and inhibiting transcription, translation, and replication. Furthermore, some NPs, such as silver, have a greater affinity for phosphorus and sulfur, which causes them to bond specifically with macromolecules containing phosphorus, such as DNA and RNA, and membrane proteins containing sulfur. This breaks down nucleic acids and prevents protein synthesis, which disrupts the regular operation the bacterial cell and leads to its death[6,13–16].

The main aim of this study is to synthesize green and Ag-doped ZnO NPs using *A. absinthium* extract as a reducing and capping agent. Additionally, pure ZnO NPs were prepared for a comparison. The NPs were prepared then verified using Fourier transform infrared (FTIR), X-ray diffraction (XRD), morphological scanning electron microscopy (SEM), energy dispersive spectrum (EDX), and surface area (BET) analyses. The antioxidant effect was evaluated using the DPPH assay as a colorimetric technique. The antibacterial activity of the ZnO NPs was studied using Gram-positive (*Staphylococcus aureus* ATCC 6538 and *Bacillus subtilis* ATCC 6633) and Gram-negative (*Pseudomonas aeruginosa* ATCC 9027) bacteria and gentamycin as a positive control.

2. Materials and Methods

2.1. Materials

Zinc nitrate hexahydrate ($Zn(NO_3)_2{\cdot}6H_2O$) was purchased from LOBA chemie, potassium hydroxide (KOH) from Techno Pharmchem, Bahadurgarh, India, and silver nitrate ($AgNO_3$) from Alfa Aesar company, Ward Hill, Massachusetts, United states. The *Artemisia absinthum* leaf extract and all the solutions were prepared using deionized water. DPPH radicals (Tokyo Chemical Industry Co., Ltd. (TCl), Tokyo, Japan) were sourced from Egypt. Dimethyl sulfoxide (DMSO) was purchased from Sigma-Aldrich, Milwaukee, United states. Mueller–Hinton Agar was purchased from Hi-media, Mumbai, India. The tested bacteria strains, *Staphylococcus aureus* ATCC 6538, *Bacillus subtilis* ATCC 6633, and *Pseudomonas aeruginosa* ATCC 9027, were obtained from Yemen Standardization, Metrology and Quality Control Organization, Sana'a, Yemen.

2.2. Methods

 doi:10.20944/preprints202411.0348.v1

2.2.1. Synthesis of Plant Extract, and Pure and Green ZnO NPs

Plant extract and pure and green ZnO NPs were prepared following the method of a previous study[17].

2.2.2. Synthesis of Ag-Doped ZnO NPs

Ultrasound was used to synthesize Ag-doped ZnO by reducing Ag^{+} ions to Ag^{0} on the surface of ZnO using *Artemisia absinthum* extract as the reducing agent. A volume of 90 mL of (0.34 M) aqueous solution of zinc nitrate ($Zn(NO_3)_2{\cdot}6H_2O$) and an amount of KOH (0.5M) were added to increase the mixture's pH to 12. While sonicating at 500 Hz, 90 mL of (0.06 M) of $AgNO_3$ for doping and 10 mL of *Artemisia absinthium* extract as a reducing agent were added. The reaction took 30 min to complete, and finally, a light gray residue (Ag/ZnO) was obtained, rinsed several times with deionized water, and then dried in a hot air oven at 90 °C. The powder samples were calcined at 500 °C in a muffle furnace for 2 h under atmospheric conditions. This method was adapted from that of El-Bindary with a few modifications[18].

2.2.3. Characterization

The KBr technique[19] was employed to determine the functional groups using Shimadzu fourier transform infrared spectrophotometer (FTIR, 4000–400 cm^{-1},fixed path length, Kyoto, Japan). An X-ray diffractometer (XRD, Rigaku, Tokyo-Japan, with K beta filter, time duration 10.000°/min, scanning range 10.0–90.0°, and operated at 40 kV, 40 mA) was used to verify the crystal size examination. The widely recognized Scherrer formula was used to calculate the average crystal size, *D*[20]:

$$D = \frac{K\lambda}{\beta \,.\cos\theta} \tag{1}$$

where K is a constant equal to 0.90; λ is the wavelength (0.154 nm); β is the full width at half maximum (FWHM) in radians; and θ is the diffraction angle. The elementary calculation was identified using EDX analysis, whereas the surface morphology of the NPs was verified using SEM (FESEM, JEOL-SEM, 6700F, Tokyo- Japan). Surface properties and pore size were determined by nitrogen desorption measured at 77 °C using a NOVA 2200e surface area analyzer[21], Durham- England.

2.2.4. Antioxidant Activity

Effect of Concentration

The antioxidant activity of pure, green, and Ag-doped ZnO NPs was determined using the free radical scavenging (DPPH) assay method, as adapted from Safawo et al.[3] with a few modifications. A fresh solution of 100 µM DPPH was prepared in DMSO. A volume of 3 mL was added to 1 mL of pure, green, and Ag-doped ZnO NP solution prepared at concentrations of 50, 100, 200, 300, and 400 µg/mL in DMSO; the mixture was kept in the dark at ambient temperature for 30 min. Then, UV–3600(Shimadz UV-Vis-NIR spectrophotometer, Tokyo- Japan with scanning range from 200 to 800 nm) at 517 nm was recorded, and DPPH scavenging activity was calculated using the following equation:

$$RSA\ (\%) = \frac{Ac - As}{AC} \times 100 \tag{2}$$

where A_c and A_s are the absorbance of the control and sample at 517 nm, respectively.

Effect of Time

A fresh solution of 0.002 g/mL of DPPH in DMSO was prepared and kept in the dark at an ambient temperature. A mass of 50 mg of the ZnO NPs was dispersed in 100 mL of DPPH in a 250 mL beaker. The reaction suspension was magnetically stirred, and at each time interval, 4 mL of the mixture solution was removed and centrifuged, and the absorbance of DPPH was measured using a

 doi:10.20944/preprints202411.0348.v1

UV–Vis spectrophotometer. The scavenging activity was determined by observing the decrease in the absorption properties of DPPH at λ max of 517 nm.

2.2.5. Antibacterial Activity

The antibacterial activity assays of the pure, green, and Ag-doped ZnO NPs were carried out using the hole plate diffusion method[22]. Three Petri dishes were pre-inoculated with the appropriate bacteria in the following manner:

A volume of 100 µL of the bacterial suspension was spread over plates containing Mueller–Hinton agar using a sterile cotton swab. Three wide holes (with diameters of 5 mm) were then made in the agar using a cork borer. The samples were dissolved in DMSO and the prepared sample solutions in different volumes (5 µL, 10 µL, 20 µL, and 30 µL) were introduced into each of the holes in appropriately labeled Petri dishes using a sterile micropipette. Gentamycin (10 µg/mg) was used as a positive control. The dishes were then incubated at 37 °C for 24 h, after which the zones of inhibition (ZOIs) were measured and recorded. The ZOI was taken to be the diameter of the zone visibly showing the absence of growth including the 5 mm well. If there was no inhibition, a value of 0 mm was assigned to the test sample[23].

3. Results and Discussion

3.1. FTIR Analysis

The FTIR technique was used to identify the functional groups of the active components found in the *A. absinthium* extract that serve as reducing and stabilizing agents in the synthesis of green and Ag-doped ZnO NPs[5]. Figure 1a,b depict the infrared spectra of the *A. absinthium* extract and the pure, green, and Ag-doped ZnO NPs. When comparing the pure, green, and Ag-doped ZnO NP spectra to the plant extract spectrum, there was a noticeable drop in the peak's intensity at about 3400 cm^{-1}. This suggests that the biomolecules associated with this functional group (OH of polyphenol-rich substances) play an essential role in reducing ZnO. The new broad absorption bands found in the range 410–440 cm^{-1} for the pure, green, and Ag-doped ZnO NPs confirmed their formation. These results are in line with those of previous studies[24].

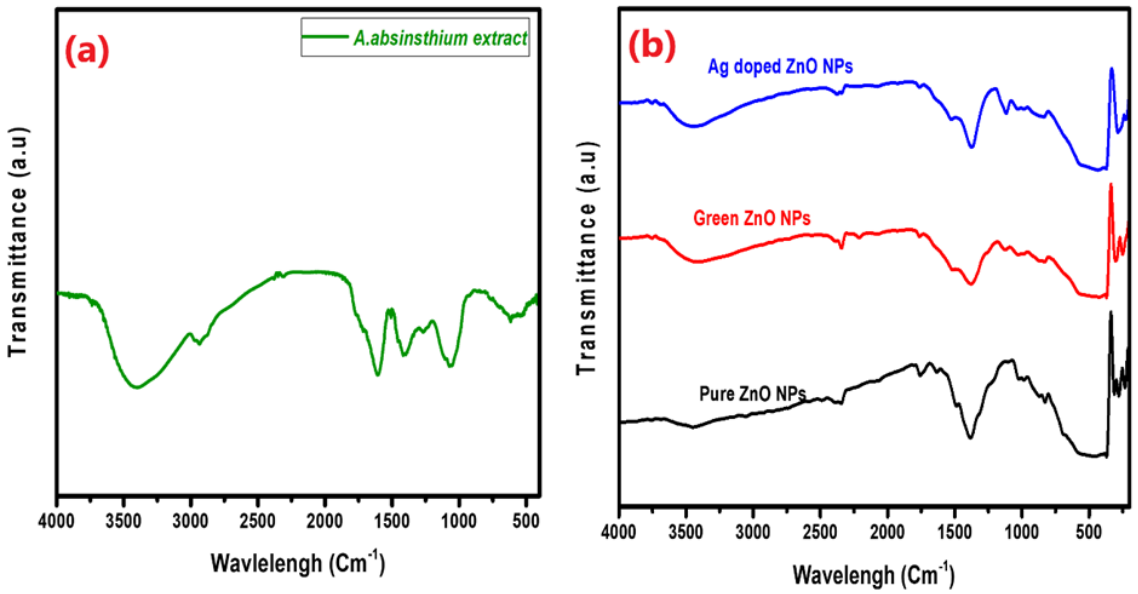

Figure 1. FTIR spectra of (**a**) *A. absinthium* extract, (**b**) pure, green, and Ag-doped ZnO NPs.

3.2. XRD Analysis

The ZnO NPs' phase purity, particle size, and crystallinity were evaluated via XRD analysis. Figure 2a displays the diffractograms of the pure, green, and Ag-doped ZnO NPs. The produced NPs showed a hexagonal wurtzite phase, with no evidence of peak impurity or a secondary phase when

 doi:10.20944/preprints202411.0348.v1

compared to the data from JCPDS Card No. 03-065-0725. Strong and narrow diffraction peaks, in particular, (100), (002), and (101), exhibit excellent crystal structure and peak intensities. Sharp extreme peaks for the pure ZnO NPs appeared at 2θ values of 31.84, 34.49, 36.32, 47.62, 56.68, 62.95, 66.48, 68.04, and 69.17, corresponding to the planes of the (100), (002), (101), (102), (110), (103), (200), (112), and (201) orientations, respectively. 2θ values for the green ZnO appeared at 31.82°, 34.47°, 36.30°, 47.60°, 56.67°, 62.93°, 68.03°, and 69.154°, corresponding to the planes of the (100), (002), (101), (102), (110), (103), (200), (112), and (201) orientations. For the Ag-doped ZnO NPs, 2θ values appeared at 31.84°, 34.49°, 36.33°, 47.62°, 56.69°, 62.95°, 66.51°, 68.03°, and 69.17°, corresponding to the planes of the following orientations: (100), (002), (101), (102), (110), (103), (200), (112), and (201), respectively.

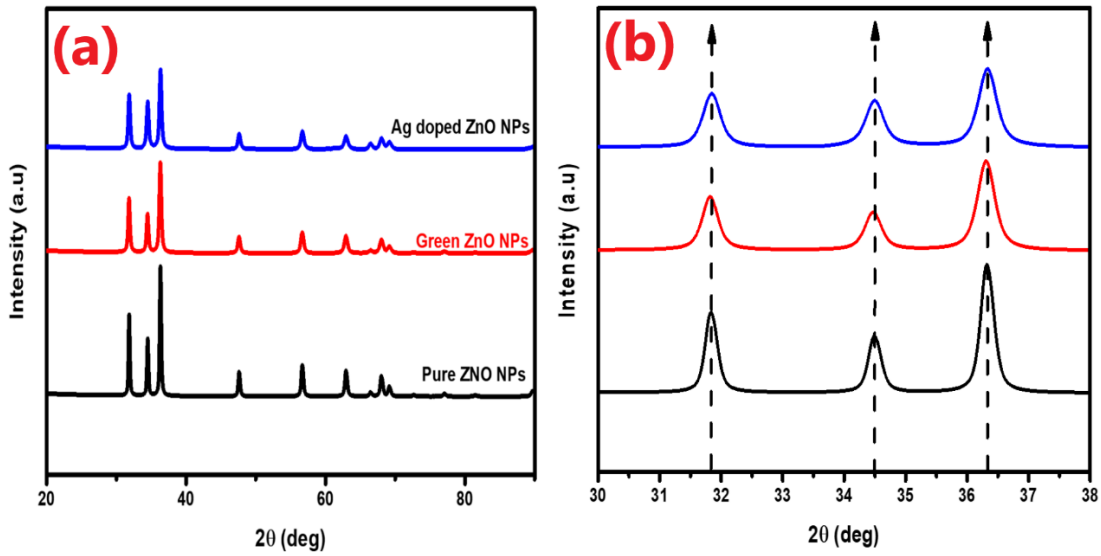

Figure 2. (**a**) XRD diffractograms of the pure, green, and Ag-doped ZnO NPs; (**b**) XRD peak shifts for pure, green, and Ag-doped ZnO NPs.

As can be seen, the diffractogram peaks of the Ag-doped ZnO exhibit increased peak intensities. This is most likely because doping improves the ZnO nanomaterial's crystallinity, which suggests that Ag NPs are growing successfully on the ZnO surface [25]. In addition, the shift in the peaks towards larger angles, as depicted in the inset of Figure 2b, is attributed to a certain degree of disorder generated by the interstitial incorporation of large-ionic-size Ag doping in the ZnO nanostructure[26].

The crystallite sizes of the pure, green, and Ag-doped ZnO NPs were calculated from the XRD data using the Scherrer formula, represented by Equation (1)[20]. The values for the pure, green, and Ag-doped ZnO were 36.32, 27.40, and 25.13, respectively. A subsequent decrease in the crystallite size was observed when the ZnO NPs were doped with Ag. The fixation of Ag ions on the surface of the ZnO NPs may be responsible for the decrease in the particle size, which in turn slows down the ZnO crystal structure's subsequent growth[26,27].

3.3. SEM/EDX Analysis

Figure 3 depicts the results of the SEM analysis. The observed results clearly show that different agglomerated particles make up both the pure and doped ZnO NPs. As shown in pictures a, c, and e, respectively, the morphological structures of the pure, green, and doped ZnO NPs have fundamentally spherical, rod-like, and hexagonal forms. The EDX spectra, as shown in Figure 3b,d,f, show sharp distinct and powerful Zn and O atom signals.

 doi:10.20944/preprints202411.0348.v1

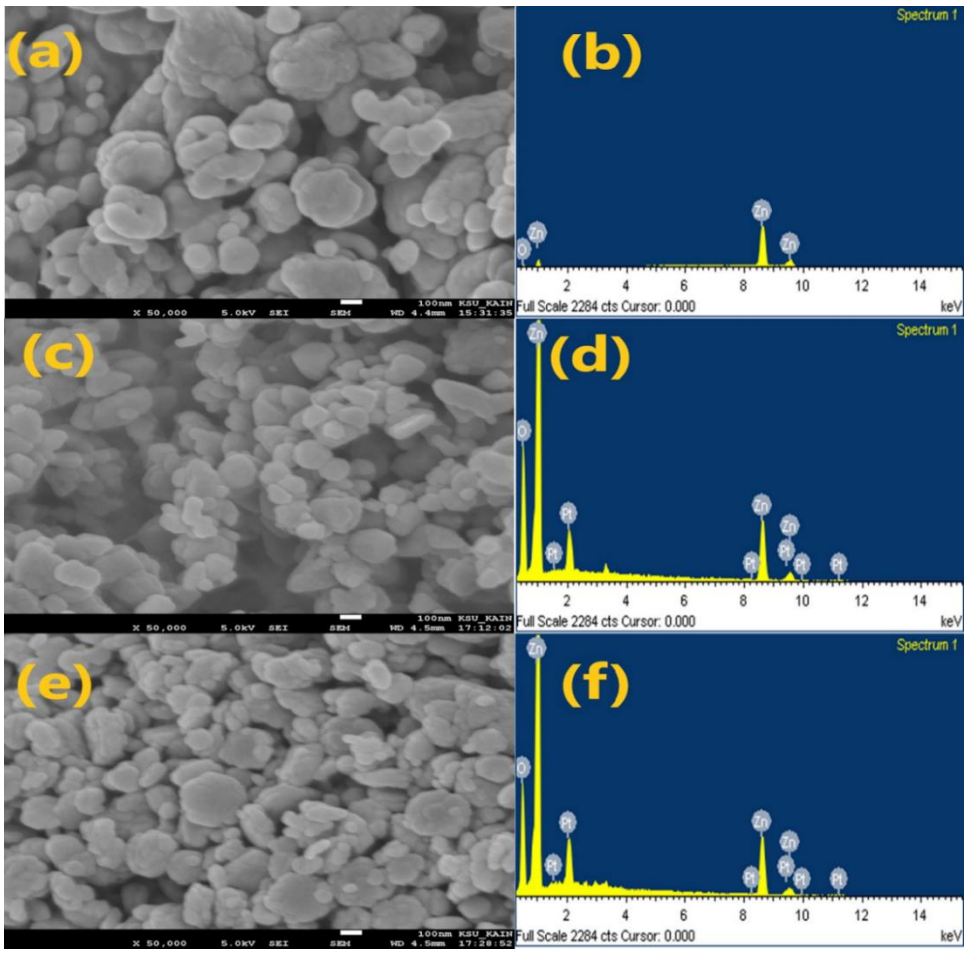

Figure 3. SEM images (a, c, d) and EDX spectra (b, d, f) counts for pure, green, and Ag-doped ZnO NPs, respectively.

3.4. BET Determination

The precise surface area of the produced nanoparticles was determined using BET. Table 1 displays the BET, pore volume, and average pore diameter of the nanomaterials. The calculated BET values were 4.003, 6.032, and 12.151 (m^2/g), where the pore volumes were 0.011, 0.017, and 0.046 (cm^3/g) for the pure, green, and Ag-doped ZnO NPs, respectively. The addition of silver to the ZnO improved the BET of the ZnO NPs. Since the Ag-doped ZnO NPs showed a large surface area, the behavior of the material as a whole began to be dominated by its surface qualities[28].

Table 1. BET, pore volume, and pore distribution of pure, biosynthesized, and Ag-doped ZnO NPs.

Samples	BET (m^2/g)	Pore Volume (cm^3/g)	Average Pore Diameter (nm)
Pure ZnO NPs	4.003	0.011	18.455
Green ZnO NPs	6.032	0.017	15.876
Ag-doped ZnO	12.151	0.046	15.882

3.5. Antioxidant Activity

The antioxidant capacity of the pure, green, and Ag-doped ZnO NPs at various concentrations (50, 100, 200, 300, and 400 µg/mL) in DMSO was measured using the DPPH assay, which is widely used to study the radical scavenging activity of green synthesized NPs[29]. Ascorbic acid was used as a standard under the same conditions. The antioxidant activity of the sample solutions was measured using UV–Vis spectrophotometry at 517 nm 30 min after the addition of DPPH in the dark at an ambient temperature. Figure 4 displays the antioxidant behavior of the Ag-doped ZnO NPs at

 doi:10.20944/preprints202411.0348.v1

different concentrations and ascorbic acid at 50 µg/mL. All the sample solutions, pure, green, and Ag-doped ZnO NPs, showed similar behavior. It is observed from the UV–Vis readings that the absorbance values of all the concentrations were almost the same. One could conclude that the ZnO NPs reached their optimum antioxidant capacity within 30 min. Figure 4B shows the antioxidant potential of the pure, green, and Ag-doped ZnO NPs and ascorbic acid at 50 µg/mL. The histogram depicts that the observed antioxidant potential of the ZnO NPs is about half the capacity of the standard ascorbic acid, with the lowest scavenging potential for the pure ZnO NPs. The higher antioxidant activity of the green and Ag-doped ZnO NPs, seen in the insert in Figure 4A,B, may be attributed to the effect of the *Artemisia absinthum* leaf extract on the green synthesized ZnO NPs' radical scavenging potential.

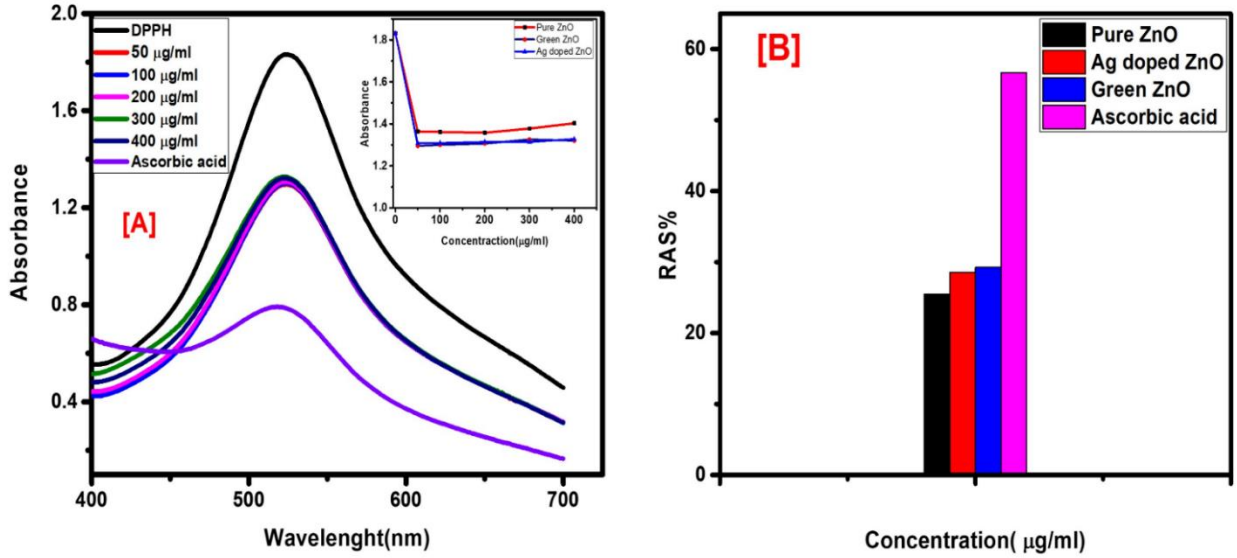

Figure 4. (**A**) Scavenging potential of pure, green, and Ag-doped ZnO NPs; (**B**) DPPH scavenging of pure, green, and Ag-doped ZnO NPs and ascorbic acid at 50 µg/mL.

Figure 5 displays the antioxidant behavior of the green and Ag-doped ZnO NPs with time. The UV–Vis readings showed a gradual decrease in the absorbance values with time, which confirmed the antioxidant activity of the ZnO NPs. A gradual change in the color of the sample solutions from deep violet to pale yellow with time was also observed. The results shown in Figure 5 show that the Ag-doped ZnO NPs reached their maximum antioxidant potential in a shorter period of time than the green ZnO NPs did. The enhanced radical scavenging activity of the Ag-doped ZnO NPs may be attributed to the effect of the large ionic size of Ag in the matrix of the ZnO nanostructure [20].

Preprints.org (www.preprints.org) | NOT PEER-REVIEWED | Posted: 5 November 2024 doi:10.20944/preprints202411.0348.v1

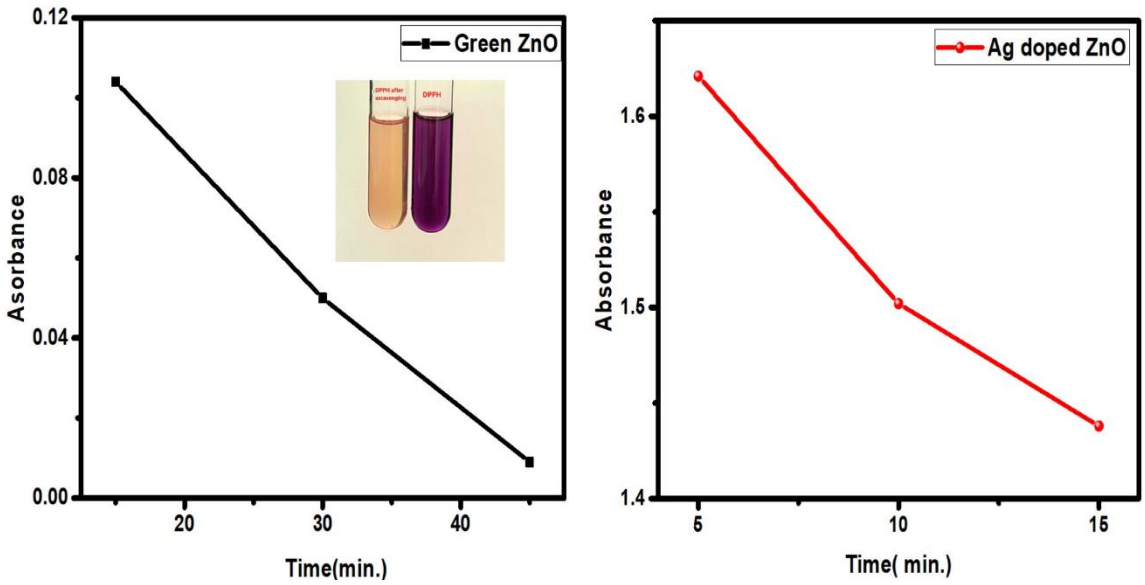

Figure 5. DPPH scavenging of green and Ag-doped ZnO NPs at different times.

3.6. Antibacterial Activities

The antibacterial activities of green ZnO and Ag-doped ZnO NPs against both Gram-positive (*Staphylococcus aureus* ATCC 6538 and *Bacillus subtilis* ATCC 6633) and Gram-negative (*Pseudomonas aeruginosa* ATCC 9027) bacteria was investigated using zone inhibition methods[22]. The antibacterial activity of the green and Ag-doped ZnO NPs against the bacteria mentioned above is presented in Figure 6. The ZOI around the sample-impregnated disk was observed to increase with an increasing sample solution level, indicating the bactericidal potential of the test compounds.

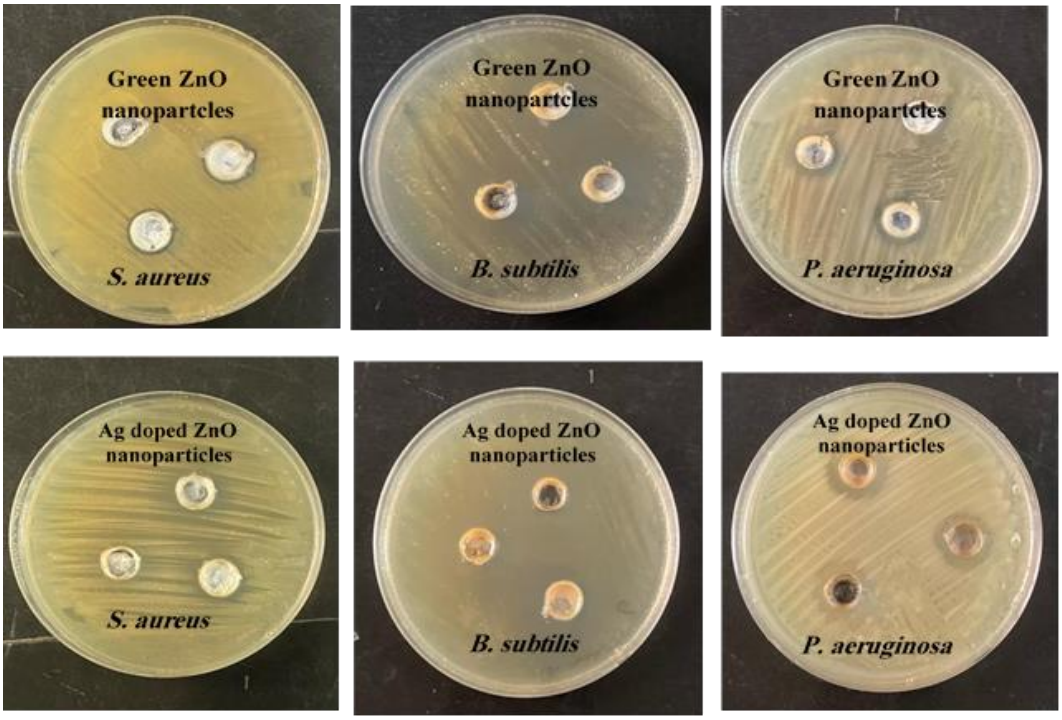

Figure 6. Antibacterial activities of ZnO nanoparticles and Ag nanoparticles synthesized using Artemisia absinthium extract.

The ZOI values of the pure, green, and Ag-doped ZnO NPs against *S. aureus*, *B. subtilis*, and *P. aeruginosa* are tabulated in Table 2. From the results obtained, the green synthesized ZnO NPs showed enhanced antibacterial activity, whereas the pure ZnO NPs showed no antibacterial activity. This

 doi:10.20944/preprints202411.0348.v1

could be attributed to the effect of the Artemisia absinthium extract as a reducing and stabilizing agent on the green ZnO NPs. The Ag-doped ZnO NPs showed a dramatic increase (by about 2-fold) in their antibacterial activity compared to that of the green ZnO NPs against all the tested bacteria. The antibacterial activities of the Ag-doped ZnO NPs were even higher than those of gentamycin (as a standard tablet). The enhanced antibacterial activity was specifically due to the presence of silver ions anchored to the ZnO nanostructure[30,31].

Table 2. Antibacterial activities of the synthesized ZnO NPs against *Staphylococcus aureus* ATCC 6538, *Bacillus subtilis* ATCC 6633, and *Pseudomonas aeruginosa* ATCC 9027 bacteria at different solution levels, with gentamycin antibiotic as a control.

No.	Bacteria	Gentamycin (μg/mg)	Pure ZnO NPs			Green ZnO NPs			Ag/ZnO NPs		
		Solution Levels (μL)	5	10	20	5	10	20	5	10	20
				30			30			30	
			ZOI (mm)								
1	*S. aureus*	2 mm	0	0	0	0	0	1	2	0	1	2	3
2	*B. subtilis*	10 mm	0	0	0	0	5	7	8	0	10	12	14
3	*P. aeruginosa*	0 mm	0	0	0	0	0	1	2	0	3	4	6

Findings from previous studies have suggested that a correlation exists between the antibacterial activity and physicochemical characteristics (such as particle size, morphology and surface defects) of ZnO NPs. Studies have indicated that the particle size is essential in achieving a better antibacterial effect. The smaller the particle size, the better the antibacterial activity. The diameter of the peptidoglycan layer in both Gram-positive and -negative bacteria cell walls is on the nanometer scale. This means that the smaller the particle size, the more easily it can interact with the cell wall and cause damage[13,16,32]. When comparing the particle size, morphology, and surface defects of the ZnO NPs, the Ag-doped ZnO NPs showed the smallest particle size, spherical rod-like shapes with the largest surface, and surface defects due to the interstitial incorporation of the Ag ions into the ZnO nanostructure. Hence, the enhanced antibacterial activity of the Ag-doped ZnO NPs is supported.

4. Conclusions

Green and Ag-doped ZnO nanoparticles were successfully synthesized through an eco-friendly method using aqueous *Artemisia absinthium* leaf extract as a reducing and stabilizing agent. Pure ZnO NPs were also synthesized without the leaf extract for comparative purposes. The prepared ZnO NPs were characterized using various analytical techniques, including XRD, SEM, EDX, UV–Vis, FTIR spectroscopy, and BET. The structural characteristics of the synthesized ZnO nanostructures confirmed that the NPs exhibited a mixture of spherical, rod-like, and hexagonal shapes. The DPPH assay indicated the antioxidant activity of the ZnO NPs with a radical scavenging potential half that of ascorbic acid. The antibacterial activity of the synthesized ZnO NPs was evaluated against three different bacterial strains: *Staphylococcus aureus* ATCC 6538, *Bacillus subtilis* ATCC 6633, and *Pseudomonas aeruginosa* ATCC 9027. This was performed using the hole plate diffusion method with different volumes (5–30 μL), and it was found that the Ag-doped ZnO NPs showed an enhanced antibacterial efficacy compared to the green ZnO NPs, specifically due to the presence of the silver ions anchored to the ZnO NPs. On the other hand, the pure ZnO NPs showed no antibacterial activity under the same conditions. Therefore, based on the obtained results, we can conclude that the synthesized ZnO NPs, and, in particular, the Ag-doped ZnO NPs, obtained using the green approach incorporating *Artemisia absinthium* leaf extract, exhibit promising antibacterial activity for future applications.

 doi:10.20944/preprints202411.0348.v1

Author Contributions: conceptualization F.N.A., Z.M.A., and F.A.A.-Y.; methodology, F.N.A, Z.M.A., E.H.L.A and F.A.A.-Y.; software, Z.M.A.; formal analysis, F.N.A. and E.H.L.A.; investigation, F.N.A., Z.M.A., and F.A.A.-Y.; resources, F.N.A., Z.M.A., E.H.L.A., and F.A.A.-Y.; data curation Z.M.A., E.H.L.A., and F.A.A.-Y.; writing—original draft preparation Z.M.A. and F.A.A.-Y.; writing—review and editing, Z.M.A., F.A.A.-Y., and T.I.H.; supervision, Z.M.A. and S.Z.A.M.; project administration, Z.M.A.; funding acquisition, F.A.A.-Y., F.N.A., Z.M.A., S.Z.A.M., and T.I.H. All authors have read and agreed to the published version of the manuscript.

Funding: This research received no external funding.

Institutional Review Board Statement: Not applicable.

Informed Consent Statement: Not applicable.

Data Availability Statement: All data are available on request.

Acknowledgments: The authors are grateful for the technical support of the Chemistry Department at the College of Science, Qassim University.

Conflicts of Interest: The authors declare no conflicts of interest.

References

1. Kazemi, S.; Hosseingholian, A.; Gohari, S.D.; Feirahi, F.; Moammeri, F.; Mesbahian, G.; Moghaddam, Z.S.; Ren, Q. Recent advances in green synthesized nanoparticles: From production to application. *Mater. Today Sustain.* **2023**, *24*, 100500. https://doi.org/10.1016/j.mtsust.2023.100500.
2. Ying, S.; Guan, Z.; Ofoegbu, P.C.; Clubb, P.; Rico, C.; He, F.; Hong, J. Green synthesis of nanoparticles: Current developments and limitations. *Environ. Technol. Innov.* **2022**, *26*, 102336. https://doi.org/10.1016/j.eti.2022.102336.
3. Safawo, T.; Sandeep, B.V.; Pola, S.; Tadesse, A. Synthesis and characterization of zinc oxide nanoparticles using tuber extract of anchote (*Coccinia abyssinica* (Lam.) Cong.) for antimicrobial and antioxidant activity assessment. *OpenNano* **2018**, *3*, 56–63. https://doi.org/10.1016/j.onano.2018.08.001.
4. Osman, A.I.; Zhang, Y.; Farghali, M.; Rashwan, A.K.; Eltaweil, A.S.; Abd El-Monaem, E.M.; Mohamed, I.M.A.; Badr, M.M.; Ihara, I.; Rooney, D.W.; et al. Synthesis of green nanoparticles for energy, biomedical, environmental, agricultural, and food applications: A review. *Environ. Chem. Lett.* **2024**, *22*, 841–887. https://doi.org/10.1007/s10311-023-01682-3.
5. Vera, J.; Herrera, W.; Hermosilla, E.; Díaz, M.; Parada, J.; Seabra, A.B.; Tortella, G.; Pesenti, H.; Ciudad, G.; Rubilar, O. Antioxidant Activity as an Indicator of the Efficiency of Plant Extract-Mediated Synthesis of Zinc Oxide Nanoparticles. *Antioxidants* **2023**, *12*, 784. https://doi.org/10.3390/antiox12040784.
6. Sampath, S.; Bhushan, M.; Saxena, V.; Pandey, L.M. Green synthesis of Ag doped ZnO nanoparticles : Study of their structural, optical, thermal and antibacterial properties. *Mater. Technol.* **2022**, *37*, 2785–2794. https://doi.org/10.1080/10667857.2022.2075307.
7. Perumal, P.; Sathakkathulla, N.A.; Kumaran, K.; Ravikumar, R.; Selvaraj, J.J.; Nagendran, V.; Gurusamy, M.; Shaik, N.; Prabhakaran, S.G.; Palanichamy, V.S.; et al. Green synthesis of zinc oxide nanoparticles using aqueous extract of shilajit and their anticancer activity against HeLa cells. *Sci. Rep.* **2024**, *14*, 2204. https://doi.org/10.5281/ zenodo. 83293 57.
8. Hairunisa, I.; Mentari, I.A.; Julianti, T.; Wikantyasning, E.R.; Cholisoh, Z.; Ningsih, S.C.; Muslim, M.R.F. Antioxidant Activities in Different Parts of Pulasan (*Nephelium mutabile* Blume) from East Borneo. *Int. Conf. Biodivers.* **2021**, *736*, 012018. https://doi.org/10.1088/1755-1315/736/1/012018.
9. Jomova, K.; Raptova, R.; Alomar, S.Y.; Alwasel, S.H.; Nepovimova, E.; Kuca, K.; Valko, M. Reactive oxygen species, toxicity, oxidative stress, and antioxidants: Chronic diseases and aging. *Arch. Toxicol.* **2023**, *97*, 2499–2574. https://doi.org/10.1007/s00204-023-03562-9.
10. Al-Tarifi, B.Y.; Mahmood, A.; Assaw, S. Comparison of Different Organic Solvents on Antioxidant Activity of Astaxanthin Extracted from Hematococcus pluvialis Using Colorimetric and Non-colorimetric Methods. *Orient. J. Chem.* **2020**, *36*, 1–8.
11. Mendes, C.R.; Dilarri, G.; Forsan, C.F.; Moraes, V. De; Sapata, R.; Renato, P.; Lopes, M.; Moraes, P.B. De; Montagnolli, R.N.; Ferreira, H.; et al. Antibacterial action and target mechanisms of zinc oxide nanoparticles against bacterial pathogens. *Sci. Rep.* **2022**, *12*, 1–10. https://doi.org/10.1038/s41598-022-06657-y.
12. Rahimi, G.; Mohammad, K.S.; Zarei, M.; Shokoohi, M.; Oskoueian, E.; Poorbagher, M.R.; Karimi, E. Zinc oxide nanoparticles synthesized using Hyssopus Officinalis L . Extract Induced oxidative stress and changes the expression of key genes involved in inflammatory and antioxidant Systems. *Biol. Res.* **2022**, *55*, 1–10. https://doi.org/10.1186/s40659-022-00392-4.

13. Nazir, A.; Akbar, A.; Baghdadi, H.B. Zinc oxide nanoparticles fabrication using Eriobotrya japonica leaves extract : Photocatalytic performance and antibacterial activity evaluation. *Arab. J. Chem.* **2021**, *14*, 103251. https://doi.org/10.1016/j.arabjc.2021.103251.
14. Hamdy, E.; Al-askar, A.A.; El-gendi, H.; Khamis, W.M.; Behiry, S.I.; Valentini, F.; Abd-Elsalam, K.; Abdelkhalek, A. Zinc Oxide Nanoparticles Biosynthesized by Eriobotrya japonica Leaf Extract: Characterization , Insecticidal and Antibacterial Properties. *Plants* **2023**, *12*, 2826. https://doi.org/10.3390/plants12152826.
15. Das, S.; Chakraborty, T. A review on green synthesis of silver nanoparticle and zinc oxide nanoparticle from different plants extract and their antibacterial activity against multi-drug resistant bacteria. *J. Innov. Pharm. Biol. Sci.* **2018**, *5*, 63–73.
16. Zhu, X.; Pathakoti, K.; Hwang, H. Green synthesis of titanium dioxide and zinc oxide nanoparticles and their usage for antimicrobial applications and environmental remediation. In *Green Synthesis, Characterization and Applications of Nanoparticles*; Ms, J., Ed.; Elsevier Inc.: Maryland Heights, MO, USA, 2019; pp. 223–263, ISBN 9780081025796.
17. Alharbi, F.N.; Abaker, Z.M.; Makawi, S.Z.A. Phytochemical Substances—Mediated Synthesis of Zinc Oxide. *Inorganics* **2023**, *11*, 328. https://doi.org/10.3390/inorganics11080328.
18. El-Bindary, A.A.; El-Marsafy, S.M.; El-Maddah, A.A. Enhancement of the photocatalytic activity of ZnO nanoparticles by silver doping for the degradation of AY99 contaminants. *J. Mol. Struct.* **2019**, *1191*, 76–84. https://doi.org/10.1016/j.molstruc.2019.04.064.
19. Rogozherov, M "Useful Tricks in KBr Tablet Technique for Recording Good Quality IR Spectra," *SSRN Electron. J.*, January, 2024. https:// doi: 10.2139/ssrn.4665789.
20. Fatimah, S.; Ragadhita, R.; Fitria, D.; Husaeni, A.; Bayu, A.; Nandiyanto, D. How to Calculate Crystallite Size from X-Ray Diffraction (XRD) using Scherrer Method. *ASEAN J. Sci. Eng.* **2022**, *2*, 65–76. https://doi.org/10.17509/xxxxt.vxix.
21. Mansour, A.T; Alprol, A. E; Shalaby, T.A; Rayan, G; Ramadan, K. M. A; and Ashour, M. "Green Synthesis of Zinc Oxide Nanoparticles Using Red Seaweed for the Elimination of Organic Toxic Dye from an Aqueous Solution," *Materials 2022*, 15, 5169. https://doi.org/10.3390/ma15155169.
22. El-Fallal, A.A; Elfayoumy, R.A; and El-Zahed, M. M. "Antibacterial activity of biosynthesized zinc oxide nanoparticles using Kombucha extract," *SN Appl. Sci.*, 2023, 5, 332. https:// doi.org/10.1007/s42452-023-05546-x.
23. Jahangirian, H.; Haron, J.; Shah, M.H. Well Diffusion Method for Evaluation of Antibacterial Activity. *Dig. J. Nanomater. Biostructures* **2013**, *8*, 1263–1270.
24. Jayachandran, A.; Aswathy, T.R.; Nair, A.S. Green synthesis and characterization of zinc oxide nanoparticles using Cayratia pedata leaf extract. *Biochem. Biophys. Rep.* **2021**, *26*, 100995. https://doi.org/10.1016/j.bbrep.2021.100995.
25. Mtavangu, S.G.; Machunda, R.L.; van der Bruggen, B.; Njau, K.N. In situ facile green synthesis of Ag–ZnO nanocomposites using Tetradenia riperia leaf extract and its antimicrobial efficacy on water disinfection. *Sci. Rep.* **2022**, *12*, 15359. https://doi.org/10.1038/s41598-022-19403-1.
26. Iqbal, Y.; Raouf Malik, A.; Iqbal, T.; Hammad Aziz, M.; Ahmed, F.; Abolaban, F.A.; Mansoor Ali, S.; Ullah, H. Green synthesis of ZnO and Ag-doped ZnO nanoparticles using Azadirachta indica leaves: Characterization and their potential antibacterial, antidiabetic, and wound-healing activities. *Mater. Lett.* **2021**, *305*, 130671. https://doi.org/10.1016/j.matlet.2021.130671.
27. Makauki, E.; Mtavangu, S.G.; Basu, O.D.; Rwiza, M.; Machunda, R. Facile biosynthesis of Ag–ZnO nanocomposites using Launaea cornuta leaf extract and their antimicrobial activity. *Discov. Nano* **2023**, *18*, 142. https://doi.org/10.1186/s11671-023-03925-2.
28. Shamhari, N.M.; Wee, B.S. Synthesis and Characterization of Zinc Oxide Nanoparticles with Small Particle Size Distribution. *Acta Chim. Slov.* **2018**, *65*. https://doi.org/10.17344/acsi.2018.4213.
29. Pavan Kumar, M.A.; Suresh, D.; Nagabhushana, H.; Sharma, S.C.; Shobharani, R..; Nethravathi, P.. Artocarpus gomezianus aided green synthesis of ZnO nanoparticles: Luminescence, Photocatalytic and Antioxidant Properties. *Spectrochim. Acta Part A Mol. Biomol. Spectrosc.* **2015**, *141*, 128–134. https://doi.org/10.1016/j.saa.2015.01.048.
30. Zarrindokht Emami-Karvani Antibacterial activity of ZnO nanoparticle on Gram-positive and Gram-negative bacteria. *African J. Microbiol. Res.* **2012**, *5*, 1368–1373. https://doi.org/10.5897/ajmr10.159.
31. Hazim, K.; Hamza, Z.; Mohamed, L.; Alyasiri, F.J. Eco-Friendly Synthesis, Antibacterial Activity, and Photocatalytic Performance of Zno Nanoparticles Synthesized via Leaves Extract of Paraserianthes Lophantha. *Pak. J. Med. Health Sci.* **2022**, *16*, 581–585. https://doi.org/10.53350/pjmhs22163581.
32. da Silva, B.L.; Caetano, B.L.; Chiari-Andréo, B.G.; Pietro, R.C.L.R.; Chiavacci, L.A. Increased antibacterial activity of zno nanoparticles: influence of size and surface modification. *Colloids Surfaces B Biointerfaces* **2019**, *177*, 440–447. https://doi.org/10.1016/j.colsurfb.2019.02.013.

 doi:10.20944/preprints202411.0348.v1

33. Okeke, I.S.; Agwu, K.K.; Ubachukwu, A.A.; Ezema, F.I. Influence of transition metal doping on physiochemical and antibacterial properties of ZnO[sbnd]Nanoparticles: A review. *Appl. Surf. Sci. Adv.* **2022**, *8*, 100227. https://doi.org/10.1016/j.apsadv.2022.100227.